Photo-induced effects in organic thin film transistors based on dinaphtho [2,3-b:2,3-f] Thieno[3,2-b] thiophene (DNTT)

Za'aba, Nor; Taylor, David

Organic Electronics

DOI:
10.1016/j.orgel.2018.10.041

Published: 01/02/2019

Peer reviewed version

Photo-induced Effects in Organic Thin Film Transistors Based on Dinaphtho [2,3-b:2',3'-f] Thieno[3,2-b'] Thiophene (DNTT)

N. K. Za'aba and D. M. Taylor*

School of Electronic Engineering,

Bangor University,

Dean Street, Bangor, Gwynedd LL57 1UT, UK

Abstract

We have investigated the photoresponse of organic thin film transistors (OTFTs) based on evaporated films of dinaphtho [2,3-b:2',3'-f] thieno[3,2-b'] thiophene (DNNT) as the active semiconductor and spin-coated polystyrene as the gate insulator. Both during illumination and in subsequent measurements in the dark after long periods under illumination, transfer characteristics shift to more positive gate voltages. The greatest photoresponse was achieved at 460 nm, near the absorption maximum of DNTT. The maximum photosensitivity and photoresponsivity measured were ~10^4 and 1.6 A/W respectively. The latter is the highest reported for an organic semiconductor on a polymeric gate insulator and by suitable adjustments to device geometry could be increased to match the highest reported, ~10^5 A/W, for organic semiconductors. Weaker responses were also obtained when exposed to light from the long-wavelength tail in the absorption spectrum. At these longer wavelengths, the response arises entirely from a shift in flatband voltage caused by deep interface trapping of photo-generated electrons. At 460 nm, however, the positive shift, ΔV_{ON}, in turn-on voltage is much greater than the shift, ΔV_T, in threshold voltage suggesting that ~3.5 x 10^{11} electrons/cm^2 are trapped at the interface at the start of the gate voltage sweep, but ~60% are neutralised by holes from the channel as the device begins to turn on. While the resulting change in subthreshold slope could be interpreted as a change in the density of states (DoS) in the DNTT, this is discounted. Gate bias stress measurements made under illumination, reveal that positive bias enhances interface electron trapping while negative bias reduces the effect owing to the simultaneous trapping of holes from the accumulation channel.

Key Words: Photosensitivity, OTFT, DNTT, Interface States

*Corresponding author email: d.m.taylor@bangor.ac.uk

1. Introduction

Organic semiconductors possess a range of attractive, commercially-exploitable electro-optical properties as exemplified by the widespread use of organic light emitting diodes in displays. Other identified application areas include photosensing [1-10], imaging arrays [11-13] and memory devices [14], all of which rely on the tailored light absorption properties and high optical sensitivity of organic semiconductors. Here we focus on the photoresponse of organic thin film transistors (OTFTs) which has been the subject of numerous publications over the last 15 years or so [1-14]. The interest arises from (a) the wavelength selectivity, (b) the gate-voltage control of sensitivity and (c) the potential for integrating OTFTs into large scale imaging arrays. Metal-insulator-semiconductor (MIS) capacitors, the core structure of OTFTs, have also been investigated as photodetectors but have been used mainly for obtaining specific information on optically induced processes occurring both in the semiconductor [15] and at the semiconductor-insulator interface [16].

The response of organic semiconductors to irradiation by light has been well-documented in the literature. Photons of energy equal to or higher than the optical bandgap of the organic semiconductor generate excitons, a fraction of which dissociate into holes and electrons at interfaces, impurities or in electric fields [17]. The subsequent device response then depends on the device structure, i.e. two terminals in photodiodes and MIS capacitors, three terminals in OTFTs, and on the magnitude and polarity of voltages applied to the device. As an example, consider an ideal, p-type OTFT in the off state, i.e. a positive voltage, V_G, applied to the gate and with a voltage, $V_D \leq 0$, applied to the drain. Under illumination, holes photo-generated in the semiconductor will flow towards the latter electrode giving rise to a photoconduction current which adds to the dark off current. Simultaneously, photo-generated electrons will be attracted to the semiconductor-insulator interface where they will become trapped in interface or bulk insulator states. Owing to their relatively low mobility, some electrons may also become trapped in localised states in the semiconductor. Electrons trapped near the source electrode will reduce the injection barrier there, encouraging further hole injection into the semiconductor [3,4,14] resulting in a positive shift of the threshold voltage, V_T. Electrons trapped in interface or insulator states will cause a positive shift, ΔV_{FB}, in the flat-band voltage resulting in an identical shift in V_T which also increases the device current [6,9,12,16,18-22]. Optically induced shifts in V_T are identified with the so-called photovoltaic effect in OTFTs.

In the on state, when both V_G and V_D are negative, similar processes will occur but to a different degree. For example, a bulk photocurrent driven by the voltage, V_D, between source and drain is still expected. Now, however, holes in the accumulation channel effectively screen the bulk semiconductor from control by the gate field. The normal channel current may also be enhanced by charge carriers generated within the accumulation region and by photo-generated electrons repelled from the interface towards the source. In the on state, therefore, interface/insulator electron trapping would not be expected. However, when a device is biased into saturation, $|V_D| > |V_G - V_T|$, the electric field in the insulator at the drain end of the channel reverses, thus encouraging interface electron trapping while discouraging hole trapping there. Furthermore, under illumination the thermal equilibrium Fermi level, E_F, splits into two quasi-Fermi levels, E_{Fe} for electrons and E_{Fh} for holes [1,16]. In the accumulation channel where the hole concentration is high, E_{Fh} will shift only slightly below E_F. Conversely, owing to the paucity of thermally generated electrons, E_{Fe} will rise significantly above E_F so that electrons photo-generated within a diffusion length of the interface will experience a higher trapping probability than in the dark as interface trap states lying between E_F and E_{Fe} become active [16]. It is possible, therefore, for photo-generated electrons to become trapped in interface states even when the device is turned on and the electrostatic conditions appear unfavourable.

The role of electron trapping in the photo-response of OTFTs has been recognised for many years. The main debate has centred on (a) the location of the electron traps i.e. in the semiconductor, in the insulator or at the interface between the two and (b) on their origin e.g. defects in the semiconductor, polar groups associated with the insulator and/or water-related –OH groups in or on the insulator surface. Not surprisingly, the dominance of one or other of these processes depends on the particular combination of semiconductor and insulator used for device fabrication.

Based on an extensive survey of the literature, Baeg et al [7] record that up to 2013 most investigations into the photoresponse of OTFTs were on devices based on SiO_2 or SiO_2 treated with a self-assembled monolayer (SAM) as the gate insulator. While a few laboratories reported very high photoresponsivities (390 to ~10^4 A/W), in most cases less than 1 A/W was achieved. The few devices incorporating a polymeric insulator yielded relatively low responsivities (1.4 - 15 mA/W). Recently, however, Milvich et al [9] reported a significantly higher responsivity, ~10^5 A/W, in OTFTs based on evaporated films of the organic semiconductor dinaphtho [2,3-b:2',3'-f] thieno[3,2-*b*] thiophene (DNTT) with reported mobility ~1.2 cm^2/Vs, but only after saturating the response during a five minute

period of illumination. It should be noted, however, that both SiO_2 and the SAM-treated AlO_x layers utilised in [9] are prone to hydroxylation by atmospheric moisture leading to an effective density of interface electron traps in excess of 10^{13} cm^{-2}. As indicated above, such states will contribute to the photovoltaic effect and an enhanced responsivity by trapping photo-generated electrons.

Despite the high mobility and good air stability of DNTT, relatively few reports have emerged to date of its use for photo-detection. Milvich et al [9] investigated the time-dependence of the shift in V_T during illumination with 461 nm light and the dependence of the drain current on optical power as a prelude to demonstrating a gesture recognition system. Yu et al [23] briefly explored the photosensitivity of their flexible DNTT OTFTs, also based on SAM-treated AlO_x. In contrast to Milvich et al [9], these yielded a relatively low responsivity of 50 A/W, even in devices in which the mobility was ~0.5 cm^2/Vs. Chu et al [12] used a high polarity biopolymer as the gate dielectric, probably the origin of the low mobility, ~0.002 cm^2/Vs, initially measured in the dark. However, the electron trapping ability of the polylactide biopolymer gave rise to an enhancement of the device current by a factor 10^4 over the dark current, presumably through the photovoltaic effect.

We have already undertaken detailed investigations [24, 25] into the effects of humidity, temperature and bias stress in DNTT OTFTs based on polystyrene as the dielectric with initial studies [26] on the optical response of DNTT devices fabricated on cross-linked tri(propylene glycol) diacrylate gate insulator buffered with a thin polystyrene layer. Here we report the results of a detailed study into the optical response of DNTT OTFTs on polystyrene, investigating the effects of illumination conditions, i.e. wavelength, optical power and applied voltages. We have also investigated the dynamic response to pulsed irradiation. The results point clearly to the roles of (i) interface electron trapping and (ii) device geometry in determining the photo-response of our devices.

2. Experimental

OTFTs were fabricated in the bottom-gate top-contact structure on a polyethylene naphthalate (PEN) substrate using three Kapton shadow masks as reported previously [25,27]. Aluminium gate electrodes were evaporated through the first mask onto the PEN substrate. Polystyrene (Sigma Aldrich, M_W = 350,000) was then spin-coated from a toluene solution (8 wt%) at 1000 rpm for 60 s onto the aluminium electrodes and heated for 10 min at 100ºC to remove residual solvent. The resulting film was typically ~1.0 μm thick with capacitance per unit area C_i ~2.37 nF/cm^2. Subsequently, a 60 nm film of DNTT was evaporated through a second mask. Finally, gold source/drain electrodes were evaporated

through the third mask, to define the channel dimensions: width, W = 2 mm with channel length, L = 150 µm.

Electrical characterization was undertaken using a source-measure unit (Keithley 2636B) to apply gate and drain voltages and for measuring the drain current, I_D. All measurements were made at room temperature under ambient atmospheric conditions with the test device placed in a cryostat located in a dark room. Monochromatic light from a xenon discharge lamp coupled to a monochromator (Jobin Yvon Triax 320) covering the range 400–700 nm was transmitted into the cryostat through a quartz window. The test device was illuminated through the DNTT film with the intensity of the light incident on the devices controlled by adjusting the exit slit and measured using a sensor (Anritsu model MA9411A1).

In a test sequence, the transfer characteristic was measured in the dark, in the linear regime (drain voltage, V_D = - 1V) with forward (20 V to -60 V) and reverse gate voltage sweeps at a rate of 0.75 V/s. Then a further transfer characteristic was measured, either during illumination with monochromatic light or following a period of light soaking with or without bias voltages applied. Following each of these measurements, the device was allowed to recover before subsequent light exposure. This was achieved by applying negative gate bias in order to release trapped electrons from the dielectric interface to recover the original transfer curve. The recovery process can take several seconds to minutes, depending on the V_T displacement caused by the illumination or excessive bias stress between each measurement. All measurements were made at room temperature with the cryostat at atmospheric pressure.

3. Results

3.1 Effect of Wavelength

Transfer characteristics of a DNTT OTFT obtained during illumination with monochromatic light are compared with the initial dark characteristic in Figure 1, where they are plotted on (a) semi-log and (b) linear scales. The intensities at each wavelength, λ, were similar for each case i.e. 460 nm, 0.31 mW/cm^2; 520 nm, 0.31 mW/cm^2; 570 nm, 0.31 mW/cm^2; 600 nm, 0.33 mW/cm^2 and 630 nm, 0.35 mW/cm^2. The inset in Figure 1(b) shows the gate-voltage-dependent mobility, μ, extracted from the drain current, I_D, using the relation [28]

$$\mu = \frac{L}{WC_iV_D} \cdot \frac{\partial I_D}{\partial V_G} . \quad (1)$$

At the highest gate voltages, the mobility tends to saturation at ~1 cm^2/Vs; a value consistent with good molecular order in DNTT deposited onto a smooth, low polarity polystyrene surface [27, 29].

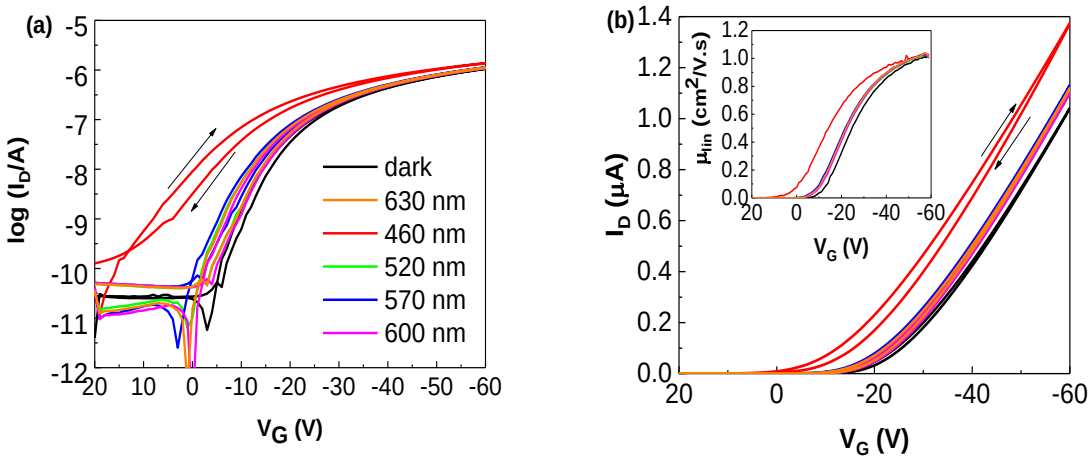

Figure 1 Transfer characteristics plotted on (a) semi-log and (b) linear scales for an illuminated device. The inset in (b) shows the corresponding gate-voltage-dependent mobility.

The corresponding plots obtained in the dark immediately after illuminating the same device for 10 mins with monochromatic light of the same intensity as above are shown in Figure 2. The off current in all the measurements, except for the reverse voltage sweep under 460 nm illumination, corresponds to the displacement current, approximately $\pm 2 \times 10^{-11}$ A, resulting from charging/discharging the gate-to-drain capacitance during the gate-voltage sweeps.

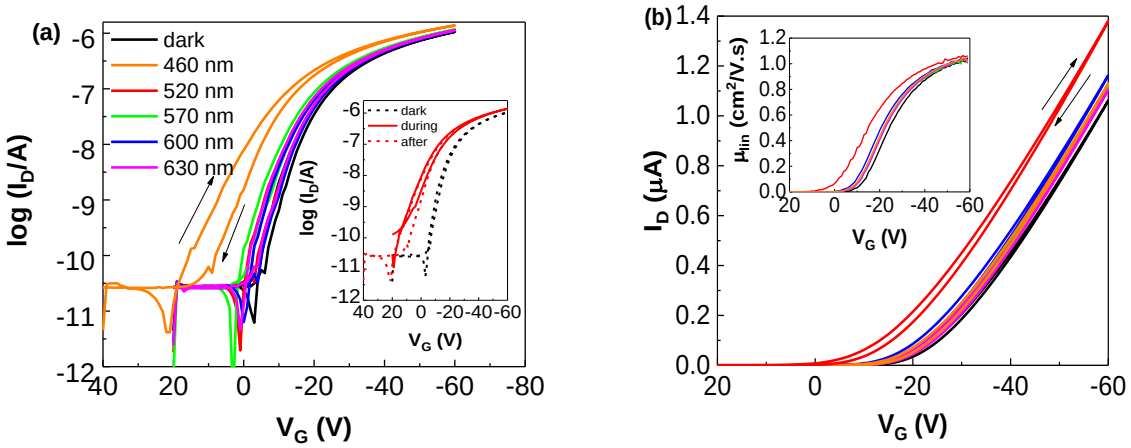

Figure 2 Post-illumination transfer characteristics plotted on (a) semi-log and (b) linear scales. The measurements were made in the dark immediately after illuminating the device for 10 mins. The inset in (a) compares the 460 nm plots obtained during and after illumination with that obtained in the dark, while that in (b) shows the corresponding gate-voltage-dependent mobility calculated from the forward transfer characteristics.

The inset in Figure 2(a) shows that the characteristics obtained both during and after illumination with 460 nm light are virtually identical except for the higher off current during the reverse voltage sweep when under illumination. At longer wavelengths the characteristics obtained after illumination were identical to those obtained during illumination (Figure S.1 in Supplementary Information).

The initial transfer characteristic obtained in the dark shows minimal hysteresis between forward and reverse gate-voltage sweeps – during the reverse sweep the plots are shifted ~1 V to more negative gate voltages leading to a slightly lower source-drain current. Except for 460 nm, a similar degree of hysteresis occurred at all wavelengths, both during and after illumination (Figure S.1 in Supplementary Information). Furthermore, in the linear plots in Figures 1 and 2, the post-irradiation characteristics are virtually identical to those obtained during illumination, all showing parallel shifts towards positive voltages. The gate-voltage-dependent mobility curves also shift in parallel towards more positive voltages with no significant change in the maximum mobility at any wavelength, as seen in the insets of Figure 1(b) and 2(b).

The effect of wavelength on the transfer characteristics obtained during the forward voltage sweep, both during and after illumination, is captured in the plots in Figure 3 which gives the changes, ΔV_T in threshold voltage and ΔV_{ON} in the turn-on voltage (defined here as the voltage at which I_D, increases above the off current). In both cases, the largest changes were obtained at 460 nm. At this wavelength, ΔV_{ON} was significantly greater than ΔV_T. This resulted in larger subthreshold slopes and a mobility rising at more positive gate voltages but increasing more slowly to its maximum value. The lower device currents during the reverse sweep also result in significant hysteresis before I_D asymptotes to a higher off current (Figure 1(a) and inset in Figure 2(a)).

3.2 Effect of Light Intensity

In this section, we report the effects of light intensity on the post-illumination transfer characteristics. The intensity at each wavelength was adjusted by controlling the exit slit of the monochromator. Although this slightly changed the breadth of the spectrum falling on the device by a few nanometres, this should have minimal effect on the device response. Transfer plots obtained for (a) 520 nm and (b) 460 nm wavelength during the forward voltage sweep are given in Figure 4 with corresponding plots for other wavelengths provided in Figure S.2 in the Supplementary Information. As the intensity increased, the above-threshold transfer characteristics shift in parallel to more positive voltages regardless of the wavelength, with the largest shifts occurring for 460 nm light (Figure S.3 in Supplementary Information). For

all wavelengths, the maximum in mobility barely changed (Figure S.2(b) in Supplementary Information).

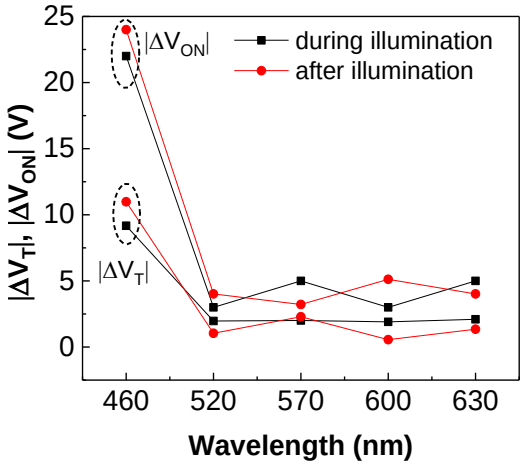

Figure 3 Effect of wavelength on the shifts ΔV_T and ΔV_{ON} observed in the threshold and turn-on voltages during forward voltage sweeps.

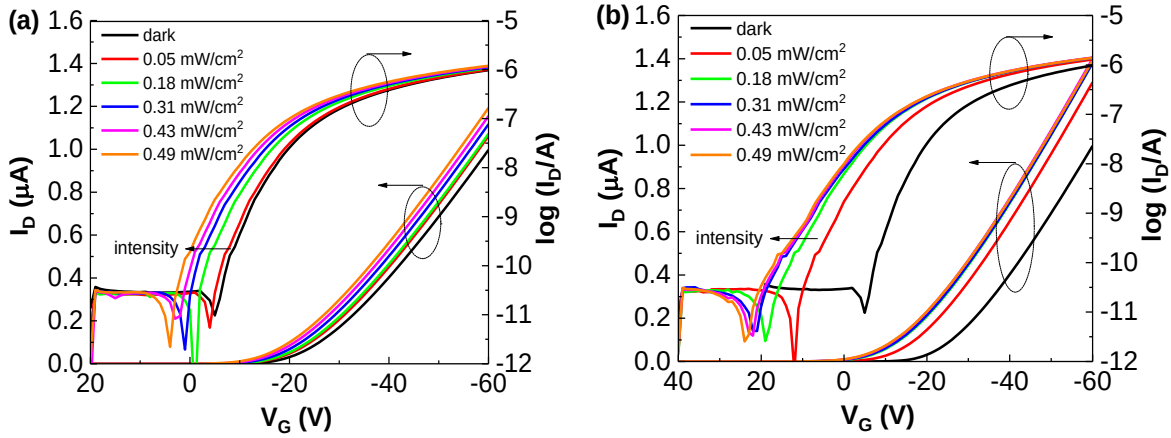

Figure 4 Effect of the intensity of (a) 520 nm and (b) 460 nm light on the forward transfer characteristics measured in the dark after illuminating the grounded device for 10 mins.

Figure 5 shows that, when $\lambda > 460$ nm, the shifts in (a) threshold voltage, ΔV_T, and (b) turn-on voltage, ΔV_{ON}, are relatively small, albeit the latter is slightly larger. For $\lambda = 460$ nm, though, both increase to saturation with the maximum in ΔV_{ON} (~28 V) much greater than that in ΔV_T (~10 V).

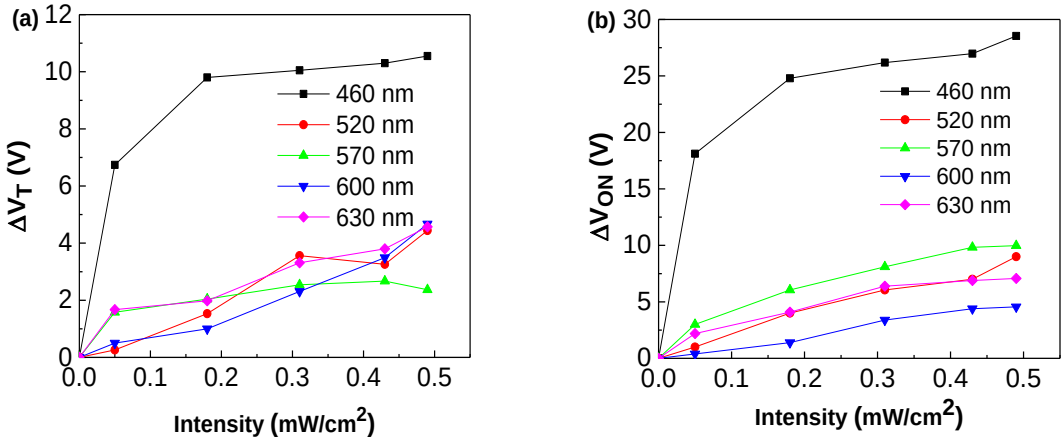

Figure 5 Changes in (a) threshold voltage, ΔV_T, and (b) turn-on voltage, ΔV_{ON}, as a function of illumination intensity. All characteristics were obtained in the dark after illumination at a particular wavelength for 10 mins.

3.3 Photosensitivity and Photoresponsivity

Two figures of merit used to quantify the optical response of phototransistors are photosensitivity, *P*, and photoresponsivity, *R*, which are expressed as:

$$P = \frac{I_{D(light)} - I_{D(dark)}}{I_{D(dark)}} \quad (2)$$

$$R = \frac{I_{D(light)} - I_{D(dark)}}{P_{OPT} A}. \quad (3)$$

Here $I_{D(light)}$ and $I_{D(dark)}$ are the drain currents measured at a given gate voltage under illumination and in the dark respectively, P_{OPT} is the power per unit area of the incident light and *A* (= W.L) the effective device area [1, 30].

Plots of photosensitivity, *P*, versus V_G for different wavelength are given in Figure 6 (a) during and (b) after illumination. The highest value of ~10^4 occurs at 460 nm and is two orders of magnitude greater than for longer wavelengths. For all wavelengths, though, a maximum occurs in the photosensitivity at V_G = -3.0 V which is close to V_{ON} in the initial dark transfer plot. As V_G sweeps to more negative voltages, *P* decreases as the number of field-induced charge carriers in the channel increases the dark on current, $I_{D(dark)}$.

In Figure 7 are plots of photoresponsivity, *R*, (a) during and (b) after illumination as a function of V_G for different wavelengths. All increase monotonically to a maximum value, with the response to 460 nm light being the greatest, reaching 0.35 A/W when the transistor is turned on fully.

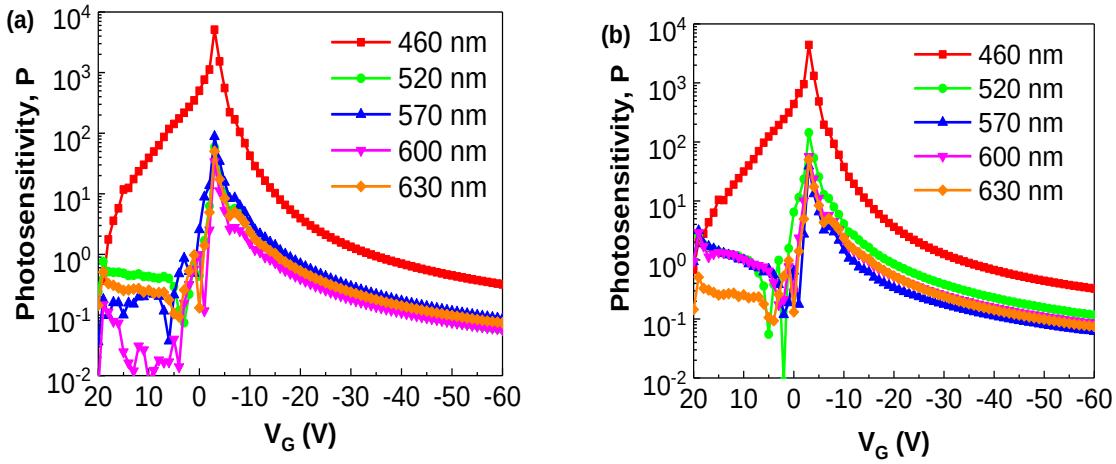

Figure 6 Photosensitivity, *P*, of a PS-DNTT OTFT (a) during and (b) after illumination. The values were extracted from the forward transfer plots in Figure 1and 2 using equation (2). Light intensity at the different wavelengths was in the range 0.31 to 0.35 mW/cm^2.

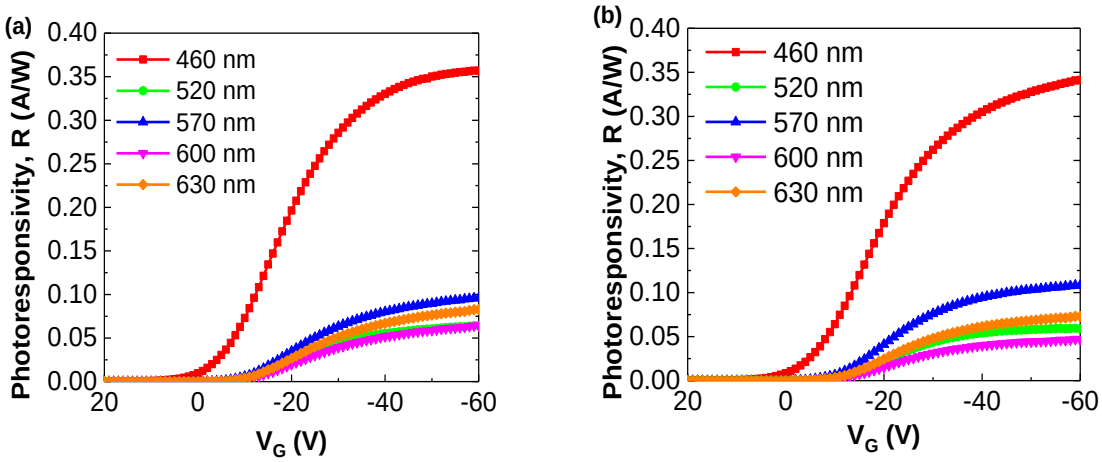

Figure 7 Photoresponsivity, *R*, of the same PS-DNTT OTFT as in Figure 6 and obtained (a) during and (b) after illumination. The values were extracted from the forward transfer plots in Figures 1 and 2 using equation (3). Light intensity at the different wavelengths was in the range 0.31 to 0.35 mW/cm^2.

The effect of changing the light intensity on (a) the maximum photosensitivity, P_{MAX}, and (b) the maximum photoresponsivity, R_{MAX}, extracted from transfer plots obtained in the dark after 10 mins irradiation is shown in Figure 8. For λ = 460 nm, P_{MAX} increases sublinearly over the whole intensity range investigated, reflecting the increasing generation rate of electron-hole pairs. At longer wavelengths, P_{MAX} is significantly lower but now increases superlinearly with increasing light intensity. At the longer wavelengths, R_{MAX} is low (<0.2 A/W) over the whole range of intensity. Interestingly, when λ = 460 nm, R_{MAX} = 1.6 A/W at the lowest intensity (0.05 mW/cm^2) but decreases inversely with increasing intensity as evidenced by the inset plot in Figure 8(b). We discuss this further in section 4.

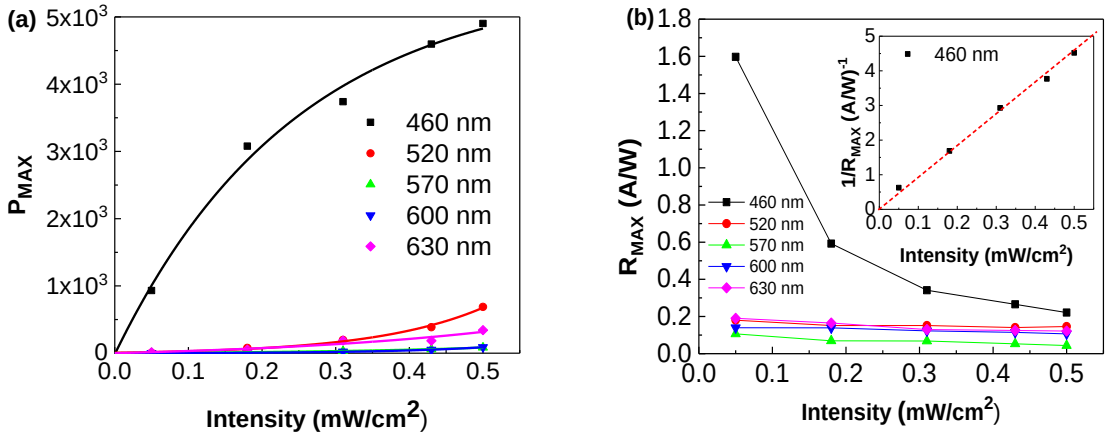

Figure 8 (a) Maximum photosensitivity, P_{MAX}, and (b) maximum photoresponsivity, R_{MAX}, of PS-DNTT OTFT as a function of intensity obtained in the dark after illuminating the device for 10 mins. The inset in (b) shows that R_{MAX} for 460 nm is inversely proportional to intensity.

3.4 Combined effect of gate bias stress and light

3.4.1 Effect of wavelength

In the above sections, devices were short-circuited during the 10-minute exposure to light. Here we explore the effect of gate bias stresses (V_G equal to -40 V or +30 V) applied during illumination. For this study the test devices, obtained from the same fabrication batch as above, were illuminated with the same wavelengths and intensities as for Figures 1 and 2. Transfer plots obtained in the dark after applying negative bias stress (NBS) while illuminating the device for 10 mins are shown in Figure 9(a). For $\lambda > 460$ nm all curves shifted negatively. Such behaviour is similar to that induced by interface hole trapping during NBS in the dark [25]. However when $\lambda = 460$ nm, the transfer characteristic shifted positively. At this wavelength, the photogeneration rate of electron-hole pairs in the DNTT is sufficiently high that electron trapping at the interface more than compensates for the hole trapping expected when the device is subjected to NBS.

The effect of positive bias stress (PBS) applied during illumination is shown in Figure 9(b). A noticeable positive shift was observed in the transfer characteristics under illumination at all wavelengths with the largest changes again seen at 460 nm.

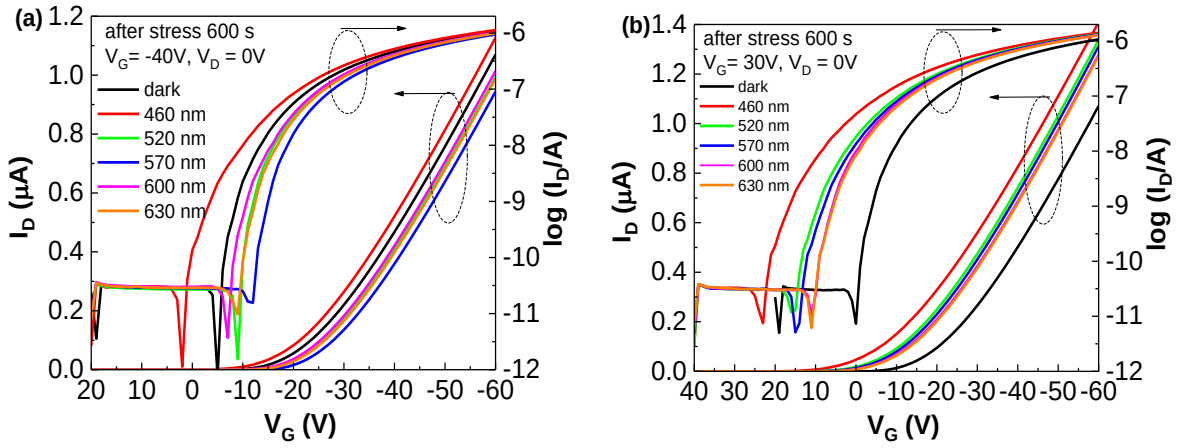

Figure 9 Transfer characteristics obtained during a forward gate voltage sweep (V_G = 20 V to -60 V) in the dark following (a) NBS: V_G = -40 V, V_D= 0V and (b) PBS: V_G = 30 V, V_D = 0 V under various illumination wavelengths**.** The intensity for different wavelengths varied between 0.31 to 0.35 mW/cm^2.

Figures 10(a) and 10(b) show the resulting changes ΔV_{ON} and ΔV_T plotted as a function of illumination wavelength. Also shown are the corresponding values obtained when devices were illuminated under short-circuit conditions. When λ = 460 nm, both ΔV_T and ΔV_{ON} were enhanced under PBS while suppressed by applying NBS. The magnitude of ΔV_{ON} was also significantly higher than ΔV_T.

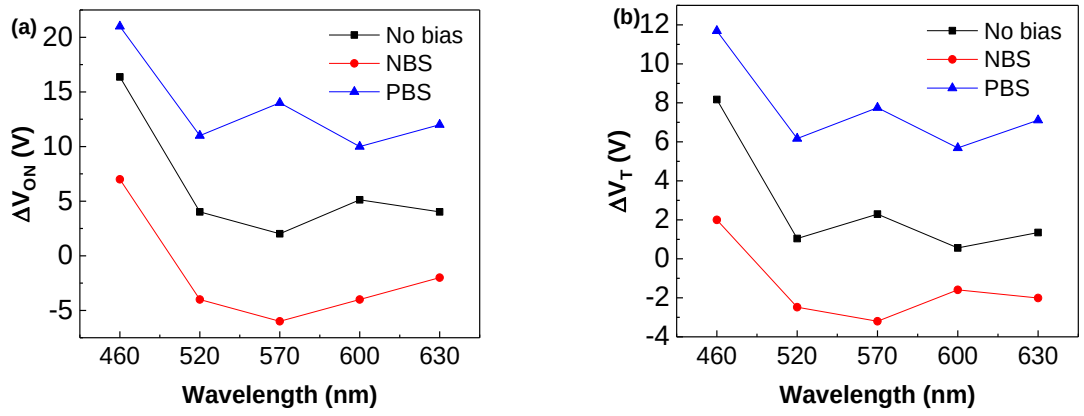

Figure 10 Shifts of (a) turn-on voltage, ΔV_{ON}, and (b) threshold voltage, ΔV_T, measured after 600 s under the combined effect of illumination and negative/positive gate bias stress as a function of wavelength.

3.4.2 *Effect of stress time*

As seen in the foregoing, the greatest optical response occurred when illuminating devices with band gap light i.e. λ = 460 nm. Accordingly, in this section the effect of stress time is investigated while illuminating with 460 nm light (0.31 mW/cm^2) in combination with NBS and PBS. Transfer characteristics were obtained during forward voltage sweeps in the dark after increasing periods of illumination under NBS and PBS. All the transfer characteristics exhibited a positive shift along the voltage axis, with changes occurring in the subthreshold slope under both stress conditions. As seen in Figure 11, the shifts ΔV_T and ΔV_{ON} induced under PBS were larger than for NBS. Under both stress conditions, the magnitude of ΔV_{ON} was significantly higher than ΔV_T.

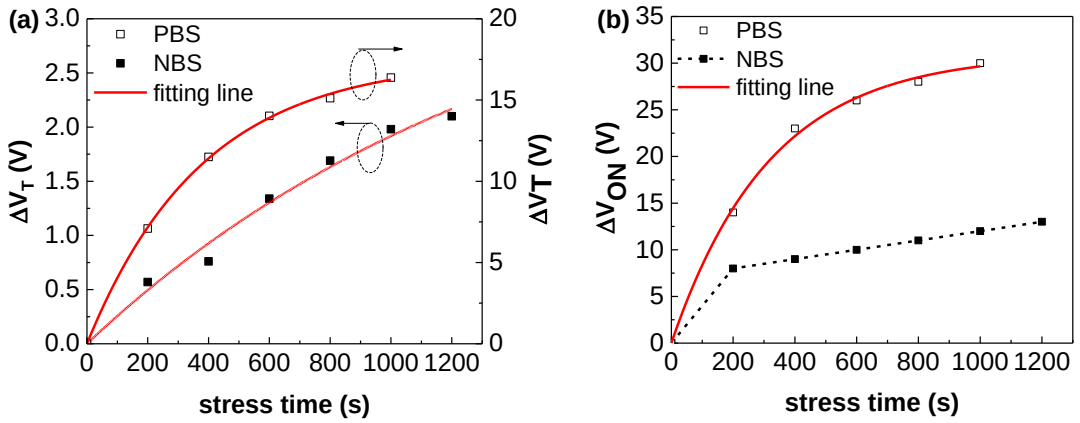

Figure 11 Shifts in (a) threshold voltage, ΔV_T and (b) turn-on voltage, ΔV_{ON} plotted as functions of stress time under illumination with 460 nm light of intensity 0.31 mA/cm^2 while also subjected to positive (V_G = 30 V) and negative (V_G = -40 V) gate bias stresses. The solid curves are exponential fits to the data using equation (7).

3.4.3 *Effect of Light Intensity*

In the previous section, the intensity of the 460 nm illumination was held constant at 0.31 mW/cm^2. Figure 12 shows the effect on ΔV_T of increasing the intensity through the range 0.05 to 0.49 mW/cm^2. Again, the device was subjected to NBS and PBS under illumination for 600 s and ΔV_T extracted from forward transfer characteristics measured subsequently in the dark. Clearly, the transfer characteristics shifted to more positive voltages as the intensity increased. As before, PBS enhances while NBS reduces the shift seen in the absence of gate bias during illumination. For the no-bias and PBS cases, ΔV_T rises rapidly with intensity but saturates above ~0.2 mW/cm^2, albeit at different values. For illumination under NBS, ΔV_T rises steadily throughout the range but remains below the no-

bias case, presumably reflecting the partial neutralisation of trapped electrons by holes from the accumulation channel.

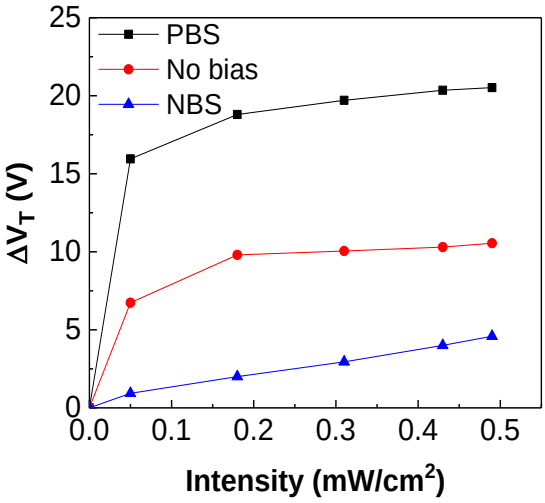

Figure 12 Shifts in threshold voltage, ΔV_T, as a function of the intensity of the 460 nm light without and with negative and positive gate bias stress.

3.5 Dynamic Photoresponse

While extracting photosensitivity and photoresponsivity from quasi-static transfer characteristics can provide figures of merit that are useful for comparing different materials systems, for most applications the dynamic response is of more interest. In the following, the photoresponse of our PS/DNTT OTFTs was investigated by switching the incident light on for 100 s and then off for 100 s and noting the changes in I_D.

Figure 13(a) shows the response of a device subjected to 630, 520 and 460 nm light pulses under positive gate voltage V_G = 5 V and with V_D = -1V, i.e. in the off state. For λ = 630 nm, no response was discernible. A weak response was observed at 520 nm. When λ = 460 nm, I_D shows a rapid initial increase (decrease) during each on(off) period, followed by a slower increase (decrease). In successive pulses, the amplitude of the response increased but on a steadily increasing background - the 100 s dark period was insufficient to return the device to the initial condition. This is an example of persistent photoconductivity reported by several others workers [31-33].

When the device was biased into the on state (V_G = -40 V, V_D = -1 V), as seen in Figure 13(b), the response to light pulses of wavelength 630 and 520 nm was relatively slow and of small amplitude. For λ = 460 nm, the response was entirely different. Now, I_D increased rapidly to an almost constant value when illuminated but decayed more slowly on

turning off the light. Furthermore, the response to successive pulses now decreased slightly on a decreasing background.

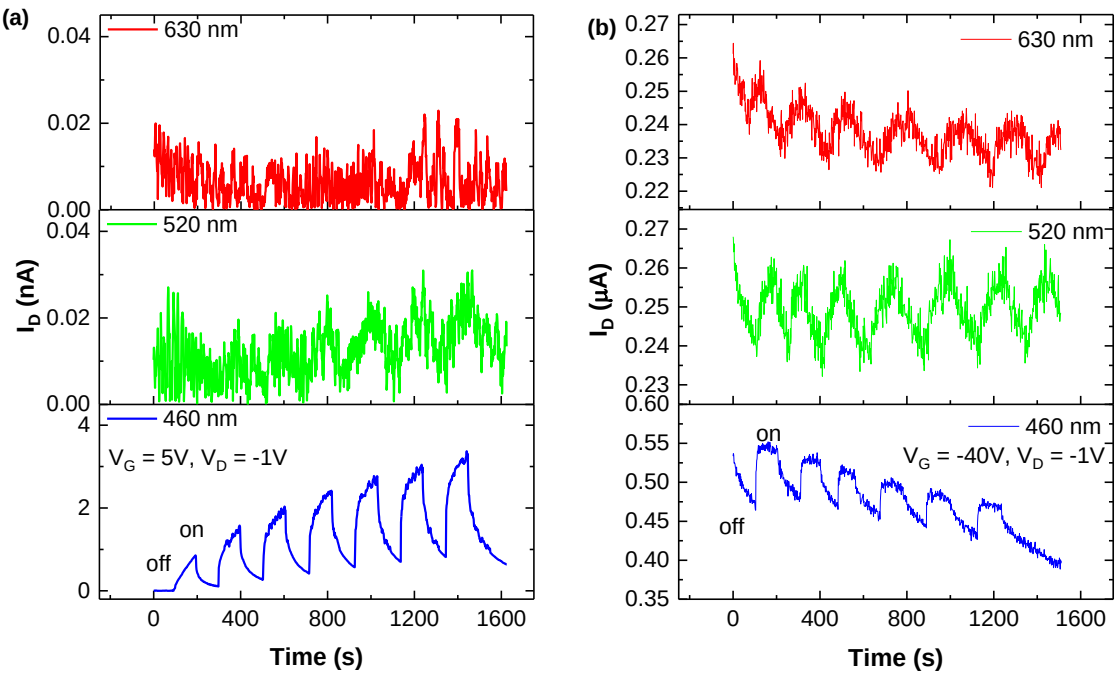

Figure 13 Time response for periodic illumination with 630, 520 and 460 nm pulses with (a) V_G = 5V, V_D = -1V and (b) V_G = -40V, V_D = -1V.

Under both bias conditions, the photosensitivity as defined by equation (2) is orders of magnitude lower than extracted from quasi-static measurements. In the following section, we argue that this result together with all those presented above, may be explained by charge trapping in interface states.

4. Discussion

In previous reports on environmental [24] and bias stress [25] effects in our OTFTs, we argued that charge trapping occurred in interface states rather than in the bulk states associated with DNTT. The main argument focused on the relative magnitudes of the contributions made to the subthreshold slope by interface and bulk states as captured in the relation [34, 35]

$$SS = \frac{kT}{q}\ln 10\left[1+\frac{q}{C_i}\left(\sqrt{\varepsilon_S N_b}+qN_{it}\right)\right] \qquad (4)$$

where k is Boltzmann's constant, T the absolute temperature, q the electronic charge, ε_S the absolute permittivity of the semiconductor, N_b the bulk density of states in the semiconductor and N_{it} the density of interface trapped charge. For physically meaningful values of N_b, SS

would be expected to be ~ 60 mV/decade, a much lower value than seen in our transfer characteristics, ~3.8 V/decade. In our case, therefore, N_{it} must dominate the value of *SS* measured from the transfer characteristics. That argument is supported here by the constancy of the maximum mobility, ~1 cm^2/Vs, measured under all conditions suggesting that no changes are occurring in either the morphology or the density of states (DoS) in the DNTT bandgap. It then follows that the large difference between V_{ON} and V_T in our devices must reflect a change in the concentration of charges trapped in interface states. We have shown in our previous publications that gold makes a good ohmic contact to DNTT and that the series resistance between the source and channel is small [36]. Also in OTFTs based on highly pure, evaporated small molecule semiconductors such as DNTT, V_{ON} corresponds to the flatband condition. To a first approximation, therefore, we may assume that the departure of V_{ON} from V_G = 0 V to slightly negative values, arises from a shift in the flatband voltage owing to trapped *holes*. In our devices V_{ON} is typically around -2 to -4 V suggesting a 'natural' interface hole trap population, $(C_i/q)\,V_{ON}$, of ~ (3 to 6) x 10^{10} cm^{-2}. However, the large negative threshold voltage, V_T ~ -27 V, coupled to almost negligible hysteresis suggests that during the gate voltage sweep, a further ~ 3.4 x 10^{11} holes cm^{-2} are trapped reversibly in interface states, effectively changing the flatband voltage during the voltage sweep. In the following, we argue that electrons photogenerated in the DNTT populate interface states and that the photoresponse is determined by the extent to which interface trapped electrons can overcome the effect of hole trapping which occurs during a gate voltage sweep.

Liguori et al [22] identify excellent light sensitivity and high mobility as the key factors in achieving a high optical response in OTFTs. The latter is confirmed in the review by Baeg et al [7] in which four out of the five highest responsivities reported (10^3 to 10^4 A/W) in the period up to 2013 were obtained from semiconductors with mobility in the range 0.4 to 1.66 cm^2/Vs, three of which were in single crystal form. As reported here and in previous publications [27, 29, 36] the hole mobility in evaporated thin films of DNTT is ~1 cm^2/Vs. DNTT also exhibits strong optical absorption in the range 275 to 480 nm with a sharp maximum close to 460 nm [9]. Also present is a weak but decreasing long-wavelength absorption tail extending beyond 700 nm.

Under illumination, both V_{ON} and V_T shift *positively* from their dark values with 460 nm light producing the biggest shifts (Figure 3), and the highest photosensitivity and photoresponsivity (Figures 6 and 7). All this supports the notion that, in the first instance, the effects observed arise from photoexcitation of electron-hole pairs in the DNTT. The weaker effects observed at longer wavelengths (Figures 1-3) are due to the release of free electrons

and holes in the sub-bandgap transitions giving rise to the long wavelength tail in the absorption spectrum. In the range 0.05 - 0.49 mW/cm^2, P_{MAX} increases with increasing intensity (Figure 8(a)), a consequence of the increased electron-hole pair generation rate. On the other hand, following illumination with 460 nm light, the changes ΔV_T and ΔV_{ON} saturate (Figure 5) while R_{MAX} decreases from its highest value (Figure 8(b)).

The maximum *positive* shift (~28 V) seen in V_{ON} corresponds to an increase $(C_i/q)\Delta V_{ON}$ ~4 x 10^{11} cm^{-2} of *electrons* trapped at the interface in states lying between E_F and E_{Fe}. The shift in V_T is less, ~10 V, suggesting that as the device turns on, and both E_F and E_{Fe} move closer to the highest occupied molecular orbital (HOMO), many of these electrons detrap or are neutralised by holes from the accumulation channel. The latter may occur either by recombination or by hole trapping in adjacent sites. The consequence is a reduction in the effective interface density of trapped electrons to ~1.5 x 10^{11} cm^{-2}. (Section S.5 in the Supplementary Information describes these processes in more detail).Without such a reduction, V_T would have reduced to ~0 V. That ΔV_T is similar both during and post illumination (Figure 3) suggests that the remaining electron population resides in deeper trap states, possibly in the gate insulator, and are inaccessible to holes from the accumulation channel during the post-illumination gate voltage sweep. Alternatively, there may be too few interface hole traps to achieve complete neutralisation. We have already shown in an earlier report [25] on bias stress measurements that the density of interface hole traps is relatively low ~10^{11} cm^{-2} in our devices. This would explain also the *positive* shifts in both ΔV_{ON} and ΔV_T when the OTFT is subjected to long periods of illumination by 460 nm light under *negative* bias stress (Figure 9(a)).

For the results extracted from post-illumination transfer characteristics, we assume that above threshold, the device current is described by the standard equation for an OTFT operating in the linear regime i.e.

$$I_D = \frac{W}{L}\mu C_i\big(V_G - (V_T(0) + \Delta V_T)\big)V_D \tag{5}$$

where $V_T(0)$ is the threshold voltage measured initially in the dark and ΔV_T the photo-induced change in threshold voltage. Substituting equation (5) into equation (3) then yields

$$R = \frac{(W/L)\mu C_i}{P_{OPT}WL}V_D\Delta V_T = \frac{\mu C_i}{L^2 P_{OPT}}V_D\Delta V_T \tag{6}$$

which shows that high mobility semiconductors should give the highest photoresponsivity as pointed out by Liguori et al [22]. (In this context, the photoresponse of OTFTs based on the recently reported thiadiazole-based polymers (mobility ~17 cm^2/Vs) [37] would be worth investigating). In the present case, Figures 1 and 2 show that μ becomes almost constant at

~1 cm^2/Vs for 50 V < $|V_G|$ < 60 V. Since photoresponsivity also saturates at R_{MAX} in this voltage range, we see from equation (6) that this must be a consequence of the saturation in ΔV_T. The parallel shifts of the above-threshold transfer plots (Figures 2 and 4) are also consistent with a constant shift in V_T. Furthermore, if μ and ΔV_T are both constant, then R_{MAX} will be inversely proportional to P_{OPT} as confirmed by the inset of Figure 8(b).

The maximum responsivity achieved here, ~1.6 A/W obtained at 50 μW/cm^2, is higher than previously reported for an organic semiconductor on a polymer gate insulator but significantly lower than ~10^5 A/W achieved for DNTT on a 3.6 nm thick SAM-treated AlO_x film [9]. However, the difference arises from the geometrical differences in the devices used. Equation (6) predicts that on reducing channel length from 150 μm in our case to 10 μm in Ref [9], R_{MAX} should increase substantially to ~360 A/W with a further increase to ~10^5 A/W achievable by increasing the gate capacitance from 2.37 nF/cm^2 in our case, to 600 nF/cm^2 as in Ref [9]. Additionally, the response of our devices is limited by the saturation of ΔV_T in Figures 5, 11 and 12, a consequence of a much lower density of deep interface electron traps, i.e. ~10^{11} cm^{-2} compared with ~10^{13} cm^{-2} in Ref [9].

If ΔV_T remains constant throughout the gate voltage sweep, then, according to equation (6) the dependence of R on V_G should follow that for mobility. In Figure 14, we see that this is true over the whole voltage range both during and after illumination with 520 nm light. Good correspondence is achieved also for $|V_G|$ > 30 V when illuminating with 460 nm light (Figure 15). However, at lower gate voltages, μ rises faster than R at 460 nm, suggesting the presence of a second mechanism in this voltage range.

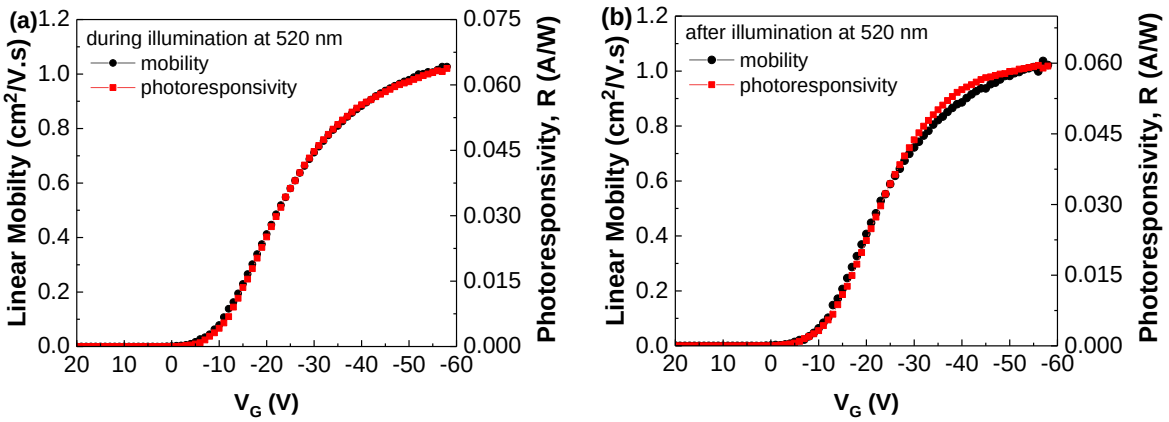

Figure 14 Gate-voltage dependence of μ and R extracted from forward transfer characteristics obtained (a) during and (b) after illumination with 520 nm light.

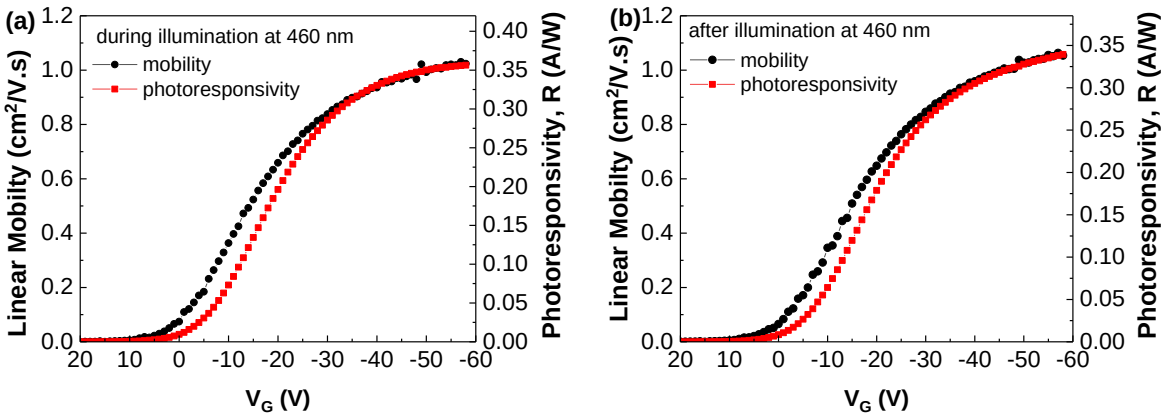

Figure 15 Gate-voltage dependence of μ and R extracted from forward transfer characteristics obtained (a) during and (b) after illumination with 460 nm light.

One possibility is that in deriving equation (6) a photoconduction component should be included in equation (5). This is unlikely to be the case. The same degree of discrepancy is present both during irradiation and afterwards in the dark. Furthermore, corresponding plots for the reverse sweep, where a delayed photoconduction component is clearly visible (Figure 1(a)), also show a similar degree of discrepancy (Figure S.4, Supplementary Information). The second, more likely, possibility is the rapid changes in flatband voltage in the sub-threshold region arising from a reduction in the interface trapped electron concentration from ~3.5 x 10^{11} cm^{-2} at V_G = 20 V to ~2 x 10^{11} cm^{-2} at V_G = 30 V when ΔV_T becomes constant at 10 V (Figure 3). The different functional dependences of μ and R on a V_G-dependent ΔV_T then explain the deviation of the two plots between 10 and -30 V.

The reduction in ΔV_T to ~10 V for $|V_G| > 30$ V is maintained during the reverse sweep, giving rise to the observed hysteresis in the transfer plots. Similar arguments apply to the post-illumination results in Figures 6 and 7, with electrons populating interface states during the period under illumination.

The results obtained after applying PBS and NBS during illumination (Figures 9-12) are readily explained as well in terms of interface charge trapping. Under illumination, the electron quasi Fermi level, E_{Fe}, rises in the bandgap [1, 16] resulting in more interface electron traps becoming active. The differences in band bending at the interface cause E_{Fe} to rise closer to the lowest unoccupied molecular orbital (LUMO) of DNTT under PBS than NBS. Furthermore, owing to the higher electric fields present within the DNTT under PBS, the exciton dissociation and hence electron-hole pair generation rates will be higher, especially at 460 nm. Consequently, illuminating under PBS is expected to lead to a more rapid increase of both ΔV_{ON} and ΔV_T to higher final values as seen in Figure 11.

The time-dependences of ΔV_{ON} and ΔV_T (except under NBS for the former) can be described by the simple-exponential function

$$\Delta V_{ON/T}(t) = \Delta V_{ON/T}(\infty)\left[1 - e^{-\left(\frac{t}{\tau}\right)}\right] \quad (7)$$

where $\Delta V_{ON/T}(\infty)$ are the changes in turn-on and threshold voltage at long times, t the duration of the stress period and τ a characteristic trapping time. The solid curves in Figure 11 show fits of equation (7) to the data using the parameters shown in Table 1. We have already shown [25] that under PBS alone $\Delta V_T(t)$ follows an exponential time-dependence. However, $\Delta V_T(\infty)$ was an order of magnitude lower and the characteristic trapping time longer, τ =520 s, consistent with the arguments above that under the combined effects of PBS and light, photo-induced electrons are more rapidly trapped in interface states that are not accessible in the dark. When the light is turned off, electrons in these states should rapidly de-trap [16]. That they do not (Figure 10), suggests that some have transferred into deeper states in the insulator.

Table 1 Parameters used to fit equation (7) to the measured ΔV_T and ΔV_{ON} in Figure 11.

Stress Conditions	$\Delta V_T(t)$		$\Delta V_{ON}(t)$	
	$\Delta V_T(\infty)$ **(V)**	τ **(s)**	$\Delta V_{ON}(\infty)$ **(V)**	τ **(s)**
PBS: V_G = +30 V, V_D = 0 V	17.5	379	31.0	318
NBS: V_G = -40 V, V_D = 0 V	3.86	1456	-	-

Interestingly, $\Delta V_{ON}(\infty)$ is close to $|V_G - V_{ON}(0)|$ suggesting that under the combined effect of illumination and gate voltage V_G = *30 V*, sufficient interface electron trapping has occurred to screen completely the DNTT from the gate field. This sets the minimum interface electron trap density at ~4.6 x 10^{11} cm^{-2}. The lower characteristic time for $\Delta V_{ON}(t)$ compared with that for $\Delta V_T(t)$ suggests that a greater number of shallower traps are involved in the former case.

As is generally found, NBS alone gives rise to hole trapping and *negative* shifts in the transfer plots which follow a stretched exponential time-dependence [25]. Under illumination with 460 nm light, though, trapping of photogenerated electrons dominates giving rise to *positive* V_T shifts of similar magnitude and with a similar characteristic time.

At longer wavelengths, the generation rate of photoelectrons is lower, the departure of E_{Fe} from its thermal equilibrium value less, so that the photo-induced positive shift in ΔV_T is lower (Figure 10) and insufficient to compensate the negative shift caused by negative gate bias stress.

These same mechanisms also explain the dynamic results presented in Figure 13. When the device is off initially (V_G = 5 V, V_D = -1 V), the response elicited by pulses of longer wavelength light is weak because the photo-induced electron generation and hence electron trapping rates are low. We concentrate, therefore, on the response to pulses of 460 nm light.

During the first 100 s exposure, I_D shows a slow increase on a timescale consistent with the early stages of the $\Delta V_{ON}(t)$ plot for PBS (Figure 11(b)). This, coupled with the value of I_D reached, ~ 1 nA, suggests that the positive shift in V_{ON} due to interface electron trapping was sufficient to begin to turn on the device, even with V_G set at +5 V. On turning off the light, a low concentration of holes is available in the channel, therefore, to recombine with some of the trapped electrons and/or to neutralise their effect by populating hole traps at the interface. This initial fast response is followed by a slower response from slow hole trapping and/or electron de-trapping, which is not complete during the 100 s period in the dark. The fast response during the second light pulse restores the final current reached during the first pulse, by replenishing the empty electron traps and/or by recombining with interface-trapped holes. The subsequent slow response is the result of further electron trapping causing V_{ON} to become even more positive. The cycle then continues. As operation moves further up the subthreshold slope due to the increasingly more positive V_{ON}, both fast and slow components increase in amplitude on a slowly rising background during successive light pulses,

Turning now to illumination of a fully turned on device (V_G = -40 V, V_D = -1 V). Pulsed illumination produces absolute changes in I_D that are significantly greater than in the off state. A clearly discernible, although sluggish, response was observed at lower wavelengths. Again we concentrate, therefore, on the sharper response to illumination with 460 nm light. Contrary to the case of an initially off device, the response to successive light pulses decreases slightly on a decreasing background. In this case, holes in the accumulation channel screen the bulk of the DNTT from the gate field, eliminating bulk photoconduction in the DNTT as the origin of the response, which if significant, would have been observed in the off device. Photoconduction in the channel could give rise to the step increases in I_D during each period of illumination. However, a more likely explanation for the almost constant amplitude of the pulsed response is a constant shift in V_T as seen in the gate-voltage-dependence of responsivity. Under illumination at the highest gate voltages, a constant positive shift occurs in V_T consistent with electron trapping in interface states lying between

E_F and E_{Fe}. In either case, the decreasing background arises from hole trapping in interface states in response to the negative gate bias stress.

As a final check that the effects we observe are related to interface states, we used the Grünewald model [24, 25, 35, 38] to extract the DoS in the DNTT from transfer characteristics obtained under different conditions. Figures S.6 – S.8 in the Supplementary Information show that, an apparent increase in the concentration of deeper states is independent of both the intensity and duration of the illumination, especially following 460 nm illumination. These features are unlikely, therefore, to be associated with bulk state creation in the DNTT. Rather, they reflect changes in the sub-threshold region of the transfer characteristic, which arise from changes in the occupancy of interface states.

5. Conclusions

We have investigated the effect of illumination on OTFTs based on DNTT as the semiconductor and polystyrene as the gate insulator. The responses obtained during illumination at a particular wavelength were similar to those obtained in the dark following a period under illumination with the device short-circuited. For $\lambda \geq 520$ nm, the transfer characteristics show parallel shifts towards more positive gate voltages, with minimal change of shape in the subthreshold region. This is readily explained by a shift in the flatband and hence threshold voltage caused by interface electron trapping, the electrons originating from those states giving rise to the sub-bandgap transitions in the optical absorption spectrum. The minimal change in the subthreshold slope had little effect on either the DoS spectrum or the gate-voltage dependence of the field-effect mobility extracted from the characteristics. For λ = 460 nm, the peak absorption in DNTT, much larger positive shifts occurred in both the threshold and turn-on voltages. Significantly, ΔV_{ON} was much greater than ΔV_T leading to an increase in the sub-threshold slope and to an apparent increase in the deeper states of the DoS spectrum. However, since the increase in deep states (a) was almost independent of light intensity and (b) had little effect on the maximum mobility extracted from the characteristics, we argue that it is not associated with the bulk states of DNTT. Rather, a high initial density of interface-trapped electrons cause the large shift, ΔV_{ON}, in the turn-on voltage, with holes neutralising a large fraction of these as the device turns on so that ΔV_T is lower. The 'deep state' features in the DoS then reflect changes in the interface state occupancy.

The effect of applying bias stress during illumination depends on both the wavelength and bias polarity. At longer wavelengths, hole trapping dominates under NBS, resulting in negative shifts in threshold voltage while electron trapping dominated under PBS. At 460 nm,

trapping of photo-induced electrons dominated irrespective of the polarity of the bias stress. We attribute this to the high electron-hole photogeneration rate leading to a higher rate of electron trapping initially in interface states lying between the thermal equilibrium Fermi level and the photo-induced electron quasi-Fermi level.

Our devices showed the highest reported responsivity, 1.6 A/W, for an evaporated organic semiconductor on a polymeric gate insulator. Although orders of magnitude lower than an earlier report on DNTT OTFTs, the difference was attributed to the differences in device geometry and the lower interface trap density in our case compared with the device based on a SAM-treated gate insulator used in the earlier study.

Finally, we showed that values of photosensitivity and photoresponsivity extracted from quasi-static characteristics are much higher than achieved in dynamic measurements, owing to the long time-constants associated with interface trapping and release.

Acknowledgements

The authors are grateful to Dr J. J. Morrison, Manchester University for supplying the DNTT sample used in this work. One of us (NKZ) wishes to thank Majlis Amanah Rakyat (MARA), Malaysia for the award of a PhD studentship.

References

[1] M.C. Hamilton, S. Martin, and J. Kanicki, IEEE Trans. Electron Dev. 51 (2004) 877-885.

[2] M.J. Deen and M.H. Kazemeini, Proc. IEEE, 93 (2005) 1312-1320.

[3] Y.-Y. Noh, D.-Y. Kim, Y Yoshida, K. Yase, B.-J. Jung, E. Lim and H.K. Shim, Appl. Phys. Lett. 86 (2005) 043501.

[4] Y.Y. Noh, D.-Y. Kim and K. Yase, J. Appl. Phys. 98 (2005) 074505.

[5] J.-M. Choi, J. Lee, D.K. Hwang, J.H. Kim, S. Im and E. Kim, Appl. Phys. Lett. 88 (2006) 043508.

[6] Y.Hu, G. Dong, C. Liu, L. Wang and Y. Qiu, Appl. Phys. Lett. 89 (2006) 072108.

[7] K.-J. Baeg, M. Binda, D. Natali, M. Caironi and Y.-Y. Noh, Adv. Mater. 25 (2013) 4267-4295.

[8] J. Kim, S. Cho, Y.-H. Kim and S.K. Park, Org. Electron. 15 (2014) 2099-2106.

[9] J. Milvich, T. Zaki, M. Aghamohammadi, R. Rödel, U. Kraft, H. Klauk and J.N. Burghartz, Org. Electron. 20 (2015) 63-68.

[10] S. Singh and Y.N. Mohapatra, J. Appl. Phys. 120 (2016) 045501.

[11] R.A. Street, M. Mulato, R. Lau, J. Ho, J. Graham, Z. Popovic and J. Hor, Appl. Phys. Lett. 78 (2001) 4193-4195.
[12] Y. Chu, X. Wu, J. Lu, D. Liu, J. Du, G. Zhang and J. Huang, Adv. Sci. 3 (2016) 1500435.
[13] A. Pierre and A.C. Arias, Flex. Print. Electron. 1 (2016) 043001.
[14] S. Dutta and K.S. Naryan, Adv. Mater. 16 (2004) 2151-2155.
[15] E.J. Meijer, A.V.G. Mangnus, B.H. Huisman, G.W. 't Hooft, D.M. de Leeuw and T.M. Klapwijk, Synth. Metal 142 (2004) 53-56.
[16] C.P. Watson, E.M. Lopes, R.F. de Oliveira, N. Alves, J.A. Giacometti and D.M. Taylor, Org. Electron. 52 (2018) 79-88.
[17] M. Weiter, V.I. Arkhipov and H. Bässler, Synth. Metals 141 (2004) 165-170.
[18] V. Podzorov and M.E. Gershenson, Phys. Rev. Lett 95 (2005) 016602.
[19] H.H. Choi, H. Najafov, N. Kharlamov, D.V. Kuznetsov, S.I. Didenko, K. Cho, A.L. Briseno and V. Podzorov, Appl. Mater. Interf. 9 (2017) 34153-34161.
[20] M. Debucquoy, S. Verlaak, S. Steudel, K. Myny, J Genoe and P. Heremans, Appl. Phys. Lett. 91 (2007) 103508.
[21] J. Kim, S. Cho, Y.-H. kim and S.K. Park, Org. Electron. 15 (2014) 2099-2106.
[22] R. Liguori, W.C. Sheets, A. Facchetti and A. Rubino, Org. Electron. 28 (2016) 147-154.
[23] F. Yu, S. Wu, X. Wang, G. Zhang, H. Luab and L. Qiu, RSC Adv., 7 (2017) 11572.
[24] N.K. Za'aba, J.J. Morrison and D.M. Taylor, Org. Electron. 45 (2017) 174-181
[25] N.K. Za'aba and D.M. Taylor, Org. Electron. (2018) 382-393.
[26] Z. Ding, G Abbas, H.E. Assender, J.J. Morrison, S.G. Yeates, E.R. Patchett and D.M. Taylor, ACS Appl. Mat. Interf. 6 (2014) 15224-15231.
[27] D.M.Taylor, E.R. Patchett, A. Williams, Z. Ding, H.E. Assender, J.J. Morrison and S.G. Yeates, Chem. Phys. 456 (2015) 85-92.
[28] D. Gundlach, L. Zhou, J. Nichols, T. Jackson, P. Necliudov, M. Shur, J. Appl. Phys. 100 (2006) 024509.
[29] G.A. Abbas, Z. Ding, H.E. Assender, J.J. Morrison, S.G. Yeates, E.R. Patchett and D. M. Taylor, Org. Electron. 15 (2014) 1998-2006.
[30] A.D. Mottram, Y.-H. Lin, P. Pattanasattayavong, K. Zhao, A. Amassian, and T.D. Anthopoulos, ACS Appl. Mat. Interf. 8 (2016) 4894-4902.
[31] P. Lutsyk, K. Janus, M. Mikołajczyk, J. Sworakowski, B. Boratyński and M. Tłaczała, Org. Electron. 11 (2010) 490-497.

[32] L. Caranzi, G. Pace, M. Sassi, L. Beverina and M. Caironi, ACS Appl. Mater. Interf. 9 (2017) 28785-28794.
[33] S. Singh and Y. Mohapatra, J. Appl. Phys, 120 (2016) 045501.
[34] A. Rolland, J. Richard, J.P. Kleider and D. Mencaraglia, J. Electrochem. Soc. 140 (1993) 3679-3683.
[35] W.L. Kalb and B. Batlogg, Phys. Rev. B 81 (2010) 035327.
[36] E.R. Patchett, A. Williams, Z. Ding, G. Abbas, H.E. Assender, J.J. Morrison, S. G. Yeates and D.M. Taylor, Org. Electron. 15 (2014) 1493-1502.
[37] J. Lee, S.-H. Kang, S.M. Lee, K.C. Lee, H. Yang, Y. Cho, D. Han, Y. Li, B.H. Lee and C. Yang, Angew. Chem. Int. Ed. 57 (2018) 13629-13634.
[38] M. Grünewald, P. Thomas and D. Würtz, Phys. Stat. Sol. 100 (1980) K139-K143.

Photo-induced Effects in Organic Thin Film Transistors Based on Dinaphtho [2,3-b:2',3'-f] Thieno[3,2-b] Thiophene (DNTT)

N. K. Za'aba and D. M. Taylor*

Supplementary Information

S.1 Comparing transfer characteristics obtained during and after illumination

In Figure S.1 we show forward and reverse transfer characteristics obtained in the dark and during illumination with 460 nm and 520 nm light. Also shown are the characteristics obtained in the dark following 10 minutes of illumination with 460 nm and 520 nm light with the device short-circuited. Illumination causes all the characteristics to shift to more positive gate voltages, with 460 nm light producing the greater effect. Importantly, the characteristics obtained during and after illumination are virtually identical except for the higher off current seen during the reverse sweep while illuminating with 460 nm light. Apart from this example of delayed photoconduction, probably in the bulk DNTT, analysis of data in the main text obtained after illumination applies also to data obtained during illumination.

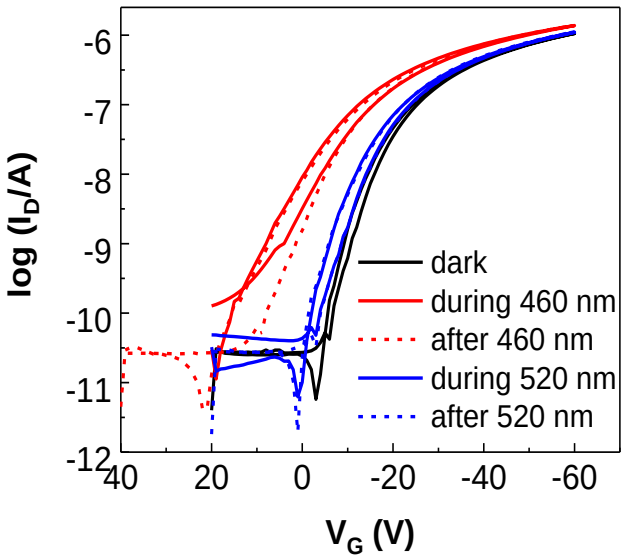

Figure S.1 Comparison of transfer characteristics obtained initially in the dark then during and after illumination with 460 nm and 520 nm light.

S.2 Effect of wavelength and light intensity

Figure S.2 shows the effect of illuminating a short-circuited device for 10 mins with light of different wavelengths and intensities. The transfer characteristics obtained subsequently in the dark are plotted on (a) semilog scales to see the subthreshold behaviour

and (b) linear scales to see the above-threshold behaviour. Also given in (b) are the gate-voltage dependences of mobility, which show that the maximum mobility is independent of wavelength and light intensity.

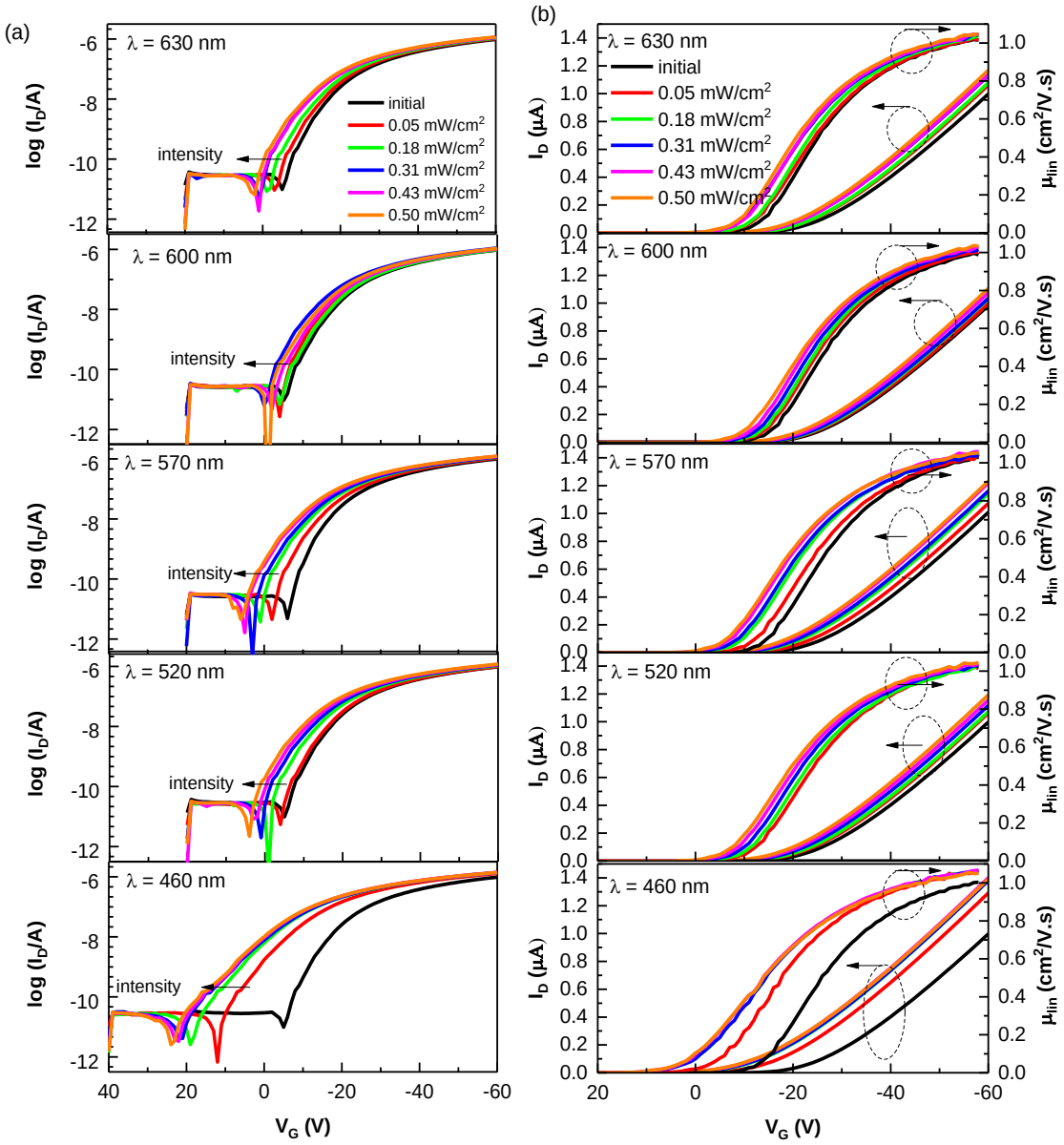

Figure S.2 Effect of different light intensities on the forward transfer characteristics measured in the dark after illuminating the grounded device for 10 mins. The data is plotted on (a) semi-log and (b) linear scales. Shown also in (b) is the gate voltage dependence of mobility.

S.3 Transfer characteristics plotted to show varying flatband voltage

Figure S.3 shows that transfer characteristics corresponding to above-threshold operation (see data plotted on linear axes) replicate the initial dark plot when shifted to

negative voltages by a fixed amount ΔV_T. While shifting the subthreshold characteristics (semi-log plots) by ΔV_{ON} corresponding to 520 nm closely follows the initial dark plot, significant departure is observed at 460 nm. That ΔV_{ON} is greater than ΔV_T suggests that the initial flatband voltage shift arising from illuminating the device in the off-state is partially relaxed above threshold – holes in the accumulation channel neutralise some of the interface trapped electrons.

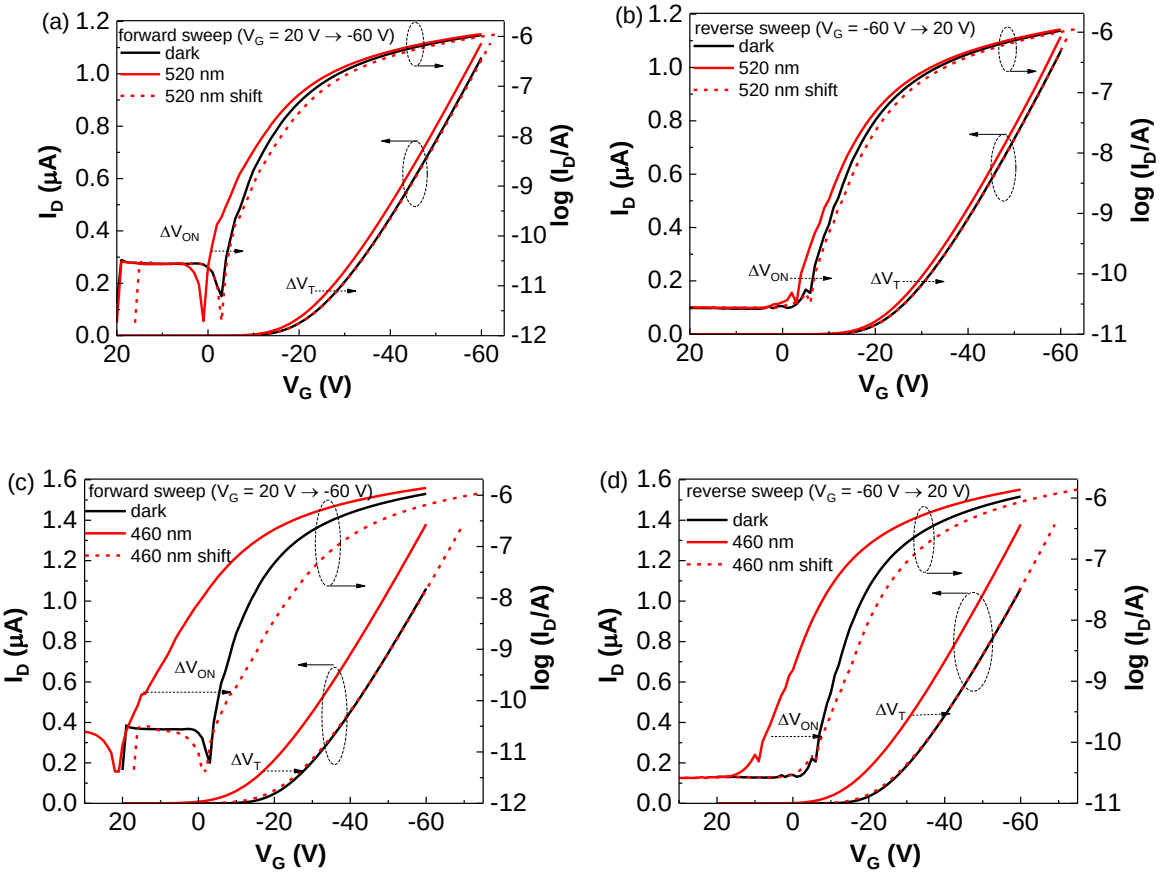

Figure S.3 Transfer characteristics in linear and semi-log scales recorded after illumination at 520 nm during (a) forward and (b) reverse gate voltage sweeps and at 460 nm during (c) forward and (d) reverse gate voltage sweeps. The dashed lines correspond to the illuminated characteristics shifted by an amount equal to the difference ΔV_{ON} and ΔV_T from the dark. The intensity for both wavelengths is 0.31 mW/cm^2.

S.4 V_G-dependence of mobility and photoresponsivity

In the main text, we compared the V_G-dependence of μ and R extracted from transfer plots obtained during the forward gate voltage sweep (20 V to -60 V). Corresponding plots for the reverse sweep in Figure S.4 show similar trends to those obtained from the forward gate voltage sweep. That is, good agreement is seen in the V_G-dependence of μ and R for 520 nm illumination with a minor differences occurring in the plots for 460 nm.

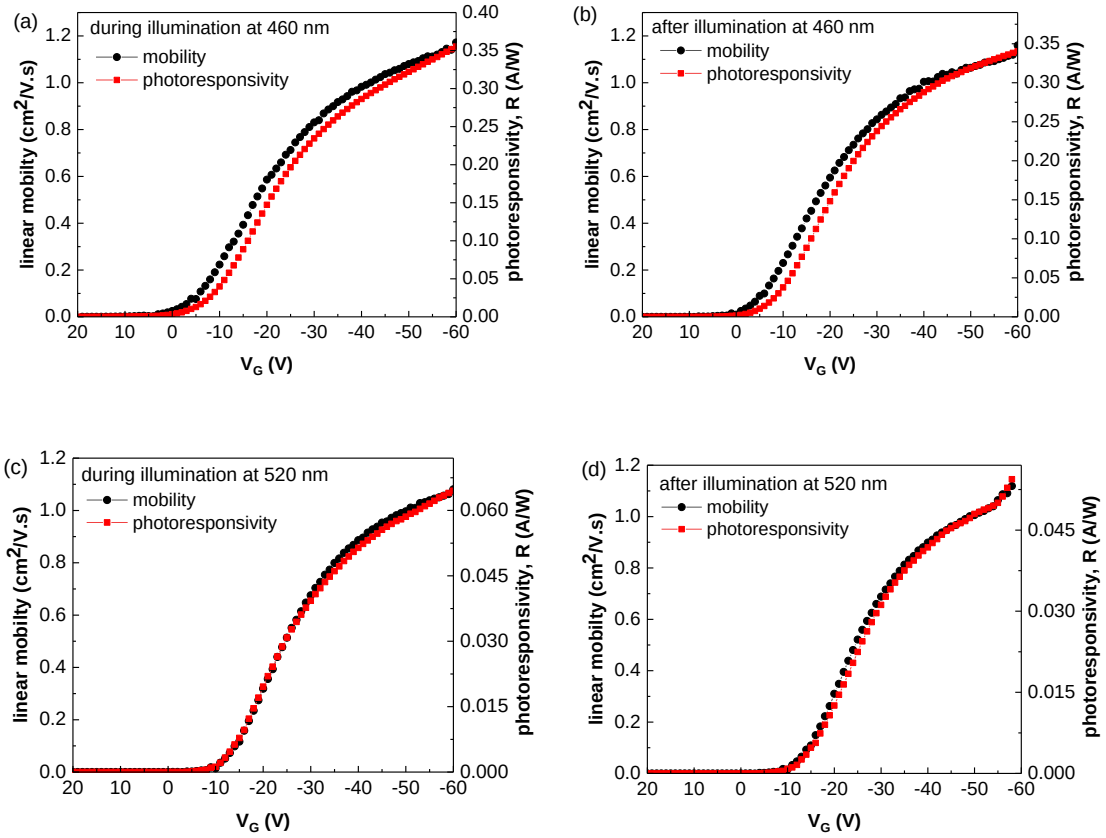

Figure S.4 Gate-voltage dependence of μ and R extracted from reverse transfer characteristics obtained (a) during and (b) after illumination with 460 nm light and (c) during and (d) after illuminating with 520 nm light.

S.5 Interface state occupancy

The density of electrons and holes trapped in interface states depends on both the energetic distribution, $N_{e/h}(E)dE$, of the traps and their probability of occupation. Since the former is unknown, we make no assumptions about the energy distribution of either the electron or hole traps which may be exponential, uniform, Gaussian or discrete, with the last possibly superimposed on one of the first three. We may, without significant error, assume a zero Kelvin Fermi function to describe the occupation of the traps as shown in Figure S.5 (a) and (b) where hole traps above and electron traps below the thermal equilibrium Fermi level, E_F, are occupied.

When the p-type OTFT is turned off, i.e. V_G is equal to, or more positive than, the flatband voltage, V_{FB}, there is likely to be an excess of trapped electrons ($V_{FB} > 0$) or trapped holes ($V_{FB} < 0$) at the interface. In our case, $V_{ON} \sim V_{FB}$ is slightly negative indicating a small excess of interface trapped holes. As the device turns on, band bending causes E_F to move closer to the valence band edge, E_V, (HOMO). As seen in Figure S.5(b), this will decrease the

trapped electron population and increase the hole population, in keeping with the experimental results.

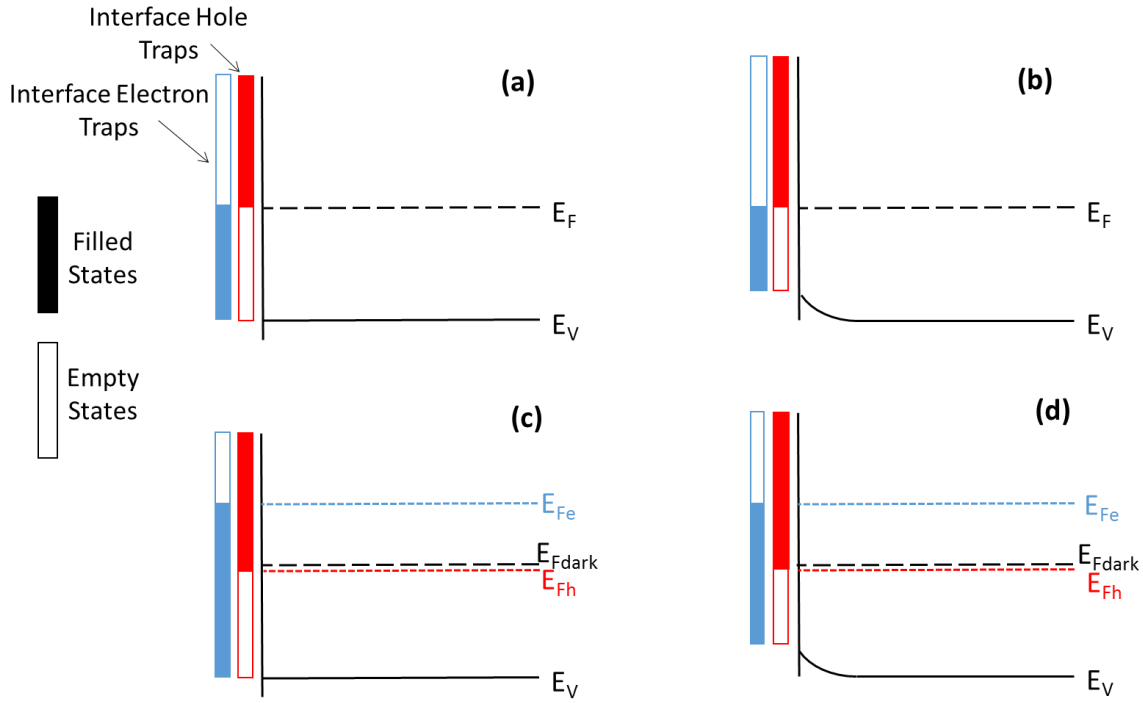

Figure S.5 Diagrams showing the occupation of interface hole and electron traps at the insulator/semiconductor interface in an OTFT under different experimental conditions. Trap occupancy assumes a zero Kelvin Fermi function. The thermal equilibrium (dark) trap occupancy is shown for a device in (a) off (flatband) and (b) on states. The corresponding situations under illumination are shown in (c) and (d).

Under illumination, E_F in the semiconductor splits into a quasi-Fermi level for electrons, E_{Fe}, and one for holes, E_{Fh}. To reflect the *relative* increases in photogenerated electrons (high) and holes (low), E_{Fe} moves further up the bandgap than E_{Fh} moves down, the latter being insignificant. When an OTFT in the off state is illuminated, and possibly immediately after depending on detrapping time constants, electron trap states lying between E_F and E_{Fe} become occupied, with holes becoming trapped in states between E_F and E_{Fh}. Our experiments show that far more electrons are trapped than holes – large positive shifts are seen in V_{ON}.

As in the dark case, when the device is turned on, band bending in the semiconductor causes the quasi-Fermi levels closer to E_V so that the concentration of interface trapped electrons decreases but that of holes increases. In our case, the interface electron population dominates even when the device is fully turned on, $\Delta V_T < \Delta V_{ON}$, suggesting that the residual

electrons are in deep traps or that there are insufficient hole traps at the interface to neutralise the excess electrons.

S.6 Density of States (DoS)

Changes observed in the subthreshold region of the transfer characteristics indicate the possibility that illumination has created new band gap states in the DNTT. To investigate this possibility, the DoS for an illuminated PS-DNTT TFT was extracted by applying the Grünewald [1,2] model to transfer plots

Figures S.6(a) and (b) give the DoS for different intensities of 460 nm and 520 nm light respectively. For λ = 520 nm the plots show almost identical distributions to the initial dark DoS, regardless of the intensity. On the other hand, for λ = 460 nm, features appearing at E-$E_V \geq 0.1$ eV which reflect significant changes in the subthreshold slope may indicate the creation of new bulk states in the DNTT. However, the DoS in this range is also independent of intensity.

Figures S.7 and S.8 show that even in the presence of positive and negative gate bias stress, the intensity of the 460 nm illumination has no effect of the resulting DoS. We conclude, therefore, that the features seen in the DoS reflect changes in the occupancy of interface states rather than changes in the DoS of DNTT as concluded in our previous reports [3,4].

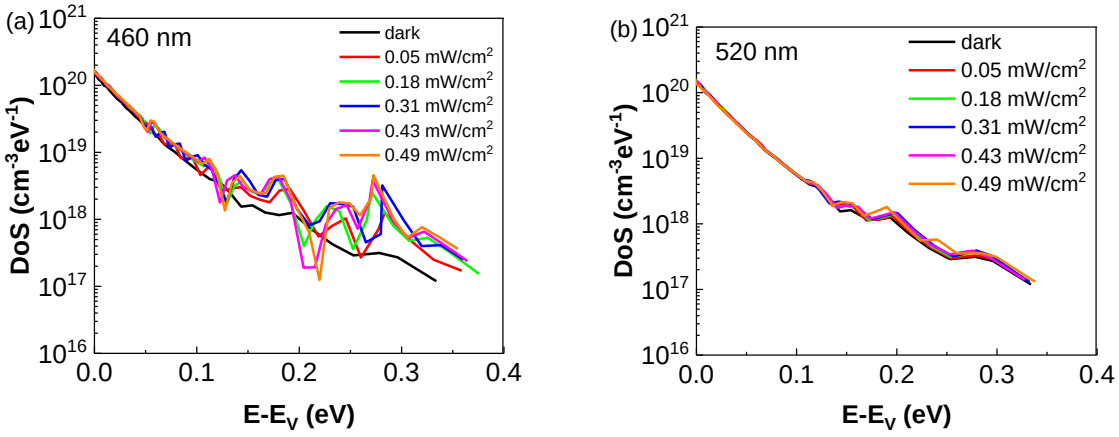

Figure S.6 DoS plots comparing the effect of light intensity at (a) 460 nm and (b) 520 nm. The plots were extracted from transfer characteristics obtained in the dark after illumination for 10 mins.

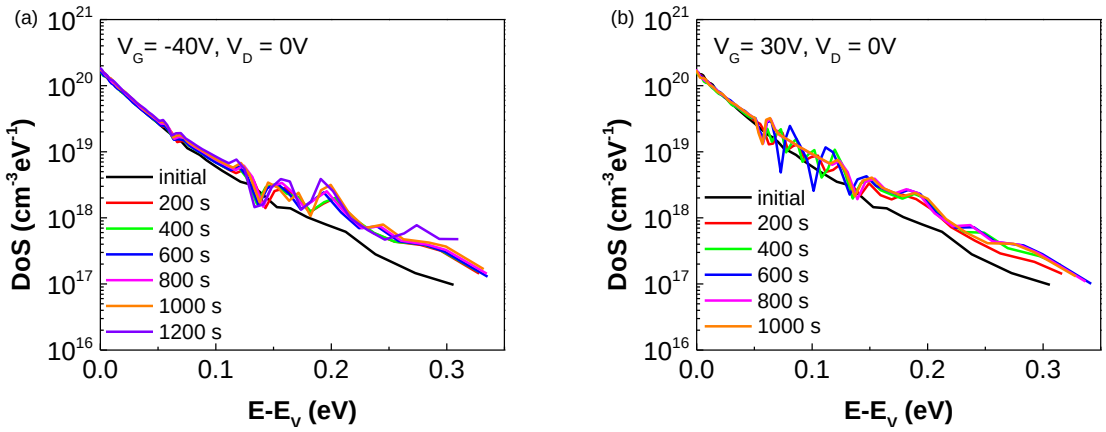

Figure S.7 DoS derived from transfer characteristics obtained in the dark after illuminating the device for increasing lengths of time with 460 nm light while under (a) NBS: V_G = -40 V and (b) PBS: V_G = 30 V. In both cases V_D = 0 V during the stress period.

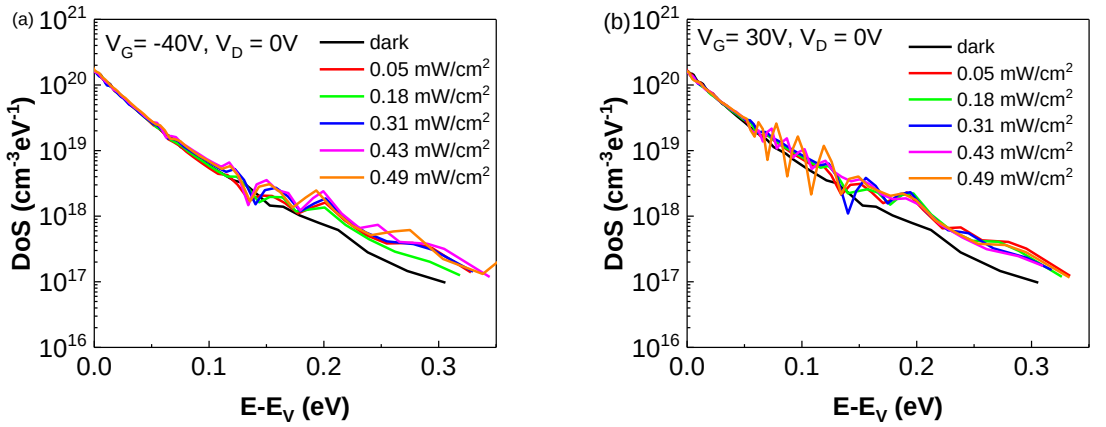

Figure S.8 DoS derived from transfer characteristics obtained in the dark after illuminating the device with 460 nm light of increasing intensity for 600 s while under (a) NBS: V_G = -40 V and (b) PBS: V_G = 30 V. In both cases V_D = 0 V during the stress period.

References

[1] W.L. Kalb and B. Batlogg, Phys. Rev. B 81 (2010) 035327.

[2] M. Grünewald, P. Thomas and D. Würtz, Phys. Stat. Sol. 100 (1980) K139-K143.

[3] N.K. Za'aba, J.J. Morrison and D.M. Taylor, Org. Electron. 45 (2017) 174-181

[4] N.K. Za'aba and D.M. Taylor, Org. Electron. (2018) 382-393.